A Quorum Sensing Active Matter in a Confined Geometry

Yuxin Zhou(周雨欣)[1], Yunyun Li(李云云)[1*], and Fabio Marchesoni[1,2*]

[1]*MOE Key Laboratory of Advanced Micro-Structured Materials and Shanghai Key Laboratory of Special Artificial Microstructure Materials and Technology, School of Physics Science and Engineering, Tongji University, Shanghai 200092, China*
[2]*Dipartimento di Fisica, Università di Camerino, I-62032 Camerino, Italy*

(Received 19 July 2023; accepted manuscript online 28 September 2023)

Inspired by the problem of biofilm growth, we numerically investigate clustering in a two-dimensional suspension of active (Janus) particles of finite size confined in a circular cavity. Their dynamics is regulated by a non-reciprocal mechanism that causes them to switch from active to passive above a certain threshold of the perceived near-neighbor density (*quorum sensing*). A variety of cluster phases, i.e., glassy, solid (hexatic) and liquid, are observed, depending on the particle dynamics at the boundary, the quorum sensing range, and the level of noise.

DOI: 10.1088/0256-307X/40/10/100505

Bacteria are capable of adjusting their motility to form large colonies, like biofilms. While motile bacteria have the advantage to swim efficiently towards food sources, biofilm aggregates are able to resist environmental threats such as antibacterial substances. Understanding the basic physical mechanisms of biofilm growth is a topic of ongoing research by many teams worldwide. Recent studies suggest that a motility-based clustering phenomenon is involved in the formation of bacterial swarms[1] and in the transition from bacterial swarms to biofilms.[2] Moreover, it is demonstrated that synthetic active materials, such as Janus colloids, can undergo motility-induced aggregation, not only via high-density steric mechanisms,[3] or lower density mutual interactions,[4] but also by simply adjusting their velocity according to the direction[5] and the local density of their peers,[6] largely insensitive to pair interactions. These situations have been modeled theoretically using both particle-based models and field theoretical approaches.[7] In that context, it was shown that the active systems may exhibit motility-induced phase separation (MIPS), whereby self-propelled particles, with only repulsive interactions, form aggregates by reducing their swimming speed in response to a local density value greater than a given threshold (a mechanism called *quorum sensing*[8,9]).

In its simplest form, MIPS has been shown to be analogous to a gas-liquid phase separation. However, recent non-equilibrium field theories have predicted intriguing behaviors, like microphase separation[10] and an active foam phase with slowly coalescing bubbles.[11] In fact, our understanding of how the microscopic details of the single-particle dynamics lead to different collective behaviors is presently far from satisfactory. Finally, it has been shown that motile *E. coli* bacteria spontaneously aggregate within minutes when subject to controlled convective flows produced by a microfluidic device.[12] It is still unclear, however, which physical ingredients are required for a minimal active-particles model to reproduce such a behavior.[13,14]

Upon a closer look, it is apparent that, while the emergence of steady aggregates of motile particles is largely driven by the nature of their mutual interactions, which ultimately influence their motility, the properties of such aggregates are strongly determined by the combined action of spatial confinement and fluctuations of both the suspension fluid and the self-propulsion mechanism. In this Letter, we revisit the model of non-reciprocal particle interaction proposed by Bechinger and coworkers[6] (also see Ref. [5]), by investigating the effects of the particle dynamics against the container walls at different noise levels. Contact and far-field reciprocal (pair) interactions have been neglected; no alignment mechanism has been invoked to trigger particle aggregation: Quorum sensing under spatial confinement is the mechanism considered here. As a result, we observe a variety of cluster phases, i.e., glassy, solid (hexatic), and liquid, and determine the relevant model phase diagram.

Model—Single Particle Dynamics. We consider the simplest realization of a synthetic microswimmer, namely a two-dimensional (2D) Janus particle (JP).[15] An active JP of label i gets a continuous push from the suspension fluid, which in the overdamped regime amounts to a self-propulsion velocity, $\boldsymbol{v}_{0i}$, with constant modulus v_0, and orientation θ_i, fluctuating with time constant τ_θ, under the combined action of thermal noise and the rotational fluctuations intrinsic to the specific self-propulsion mechanism. In two dimensions, its bulk dynamics obeys the Langevin equations[16]

$$\begin{aligned}\dot{x}_i =& v_0\cos\theta_i + \xi_{xi}(t),\\ \dot{y}_i =& v_0\sin\theta_i + \xi_{yi}(t),\\ \dot{\theta}_i =& \xi_{\theta i}(t),\end{aligned} \tag{1}$$

where $\boldsymbol{r}_i = (x_i, y_i)$ are the coordinates of the particle center of mass subject to the Gaussian noises $\xi_{pi}(t)$, with

*Corresponding authors. Email: yunyunli@tongji.edu.cn; fabio.marchesoni@pg.infn.it
© 2023 Chinese Physical Society and IOP Publishing Ltd

$\langle \xi_{qi}(t)\rangle = 0$ and $\langle \xi_{qi}(t)\xi_{pi}(0)\rangle = 2D_0\delta_{qp}\delta(t)$ for $q, p = x, y$, modeling the equilibrium thermal fluctuations in the suspension fluid. The orientational fluctuations of the propulsion velocity are modeled by the Gaussian noise $\xi_{\theta i}(t)$ with $\langle \xi_{\theta i}(t)\rangle = 0$ and $\langle \xi_{\theta i}(t)\xi_{\theta i}(0)\rangle = 2D_\theta\delta(t)$, with $D_\theta = 1/\tau_\theta$ being the relaxation rate of the self-propulsion velocity.

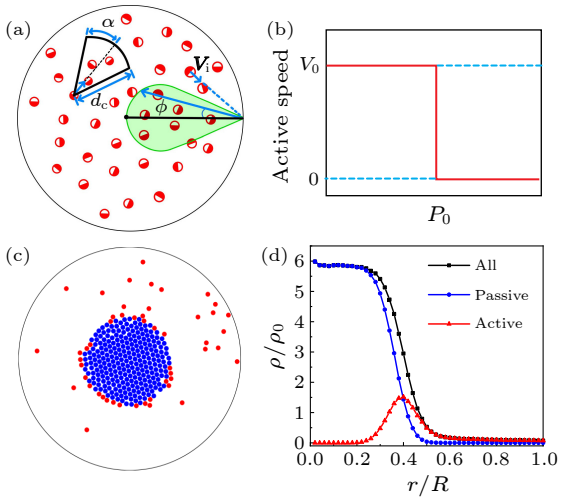

Fig. 1. Schematics of our model. (a) Illustration of the non-reciprocal interaction mechanism for N active Janus particles with visual half-angle α and horizon d_c. The distribution, $p(\phi)$, of the boundary scattering angle, Eq. (2), is plotted for $\lambda = 100$: the distance of a point on the chart line from the scattering point on the boundary is proportional to the probability that the particle gets scattered in the direction of that point. (b) Quorum sensing protocol: for values of the sensing function above the threshold $P_0(\alpha)$, Eq. (4), the particle turns from active to passive. (c) Example of passive cluster formation for $\lambda = 100$, $\alpha = (7/8)\pi$, $d_c = 16$, $D_\theta = 0.001$, $v_0 = 0.5$, $R = 45$, $r_0 = 1$, $N = 304$, and $D_0 = 0.01$ (snapshot taken at $t = 2 \times 10^4$). Active/passive particles are represented by red/blue circles. (d) Passive (blue), active (red) and total (black) radial particle distributions for the parameters in (c). These distributions have been averaged over time (10 snapshots taken every 1000 time units starting at $t = 10^4$) and initial conditions (200 realizations).

The simplifications introduced in Eq. (1) are not limited to the reduced dimensionality of the system. All noise sources have been treated independently, although strictly speaking, spatial and orientational fluctuations are statistically correlated to some degree. Moreover, we ignore hydrodynamic effects which may favor the clustering of active particles at high packing fractions. However, we make sure that the parameters used in our simulations are experimentally accessible, apparently on expressing times in seconds and lengths in microns. The stochastic differential Eq. (1) is numerically integrated by means of a standard Euler–Maruyama scheme.[17] To ensure numerical stability, the numerical integrations have been performed using an appropriately short time step, 10^{-3}.

Boundary Conditions. In this study, the JPs are confined to a restricted area, say, a circular cavity of radius R [Fig. 1(a)]. One can think of motile bacteria spreading on a Petri dish. Equation (1) still applies away from the walls; we only need to set a prescription to treat the particle collisions with the boundaries. Following Refs. [18,19], we assume that, upon hitting it, a JP is captured by the wall and immediately re-injected into the cavity, at an angle ϕ with respect to the radius (i.e., the perpendicular) through the collision point [Fig. 1(a)]. A finite (short) trapping time does not affect the conclusions of the present work. A commonly accepted distribution for such a boundary scattering angle is[18]

$$p(\phi) = 2\exp(\lambda\cos\phi)/[\pi I_0(\lambda)], \tag{2}$$

where I_0 is the modified Bessel function of the first kind, and the parameter λ depends on the temperature and the physio-chemical properties of the particle and the cavity wall. Notice that in the limit $\lambda \to \infty$ we recover the reflecting boundary conditions adopted in Ref. [6], namely, $p(\phi) = \delta(\phi)$. We consider other cavity geometries as well; an example is discussed at the bottom of the forthcoming section.

Non-Reciprocal Interaction (Sensing). When N is unchanged, independent active particles of Eq. (1) are confined into the cavity, interactions among them cannot be neglected. In our simulations we consider only two kinds of interactions: (i) *hard-core repulsion*, whereby the particles are modeled as hard discs of radius r_0. Further reciprocal interactions have been discarded; (ii) *neighbor perception*, a mechanism governing the motility of each particle depending on the spatial distribution of its neighbors. In biological systems this process is mediated by some form of inter-particle communication (mostly chemical in bacteria colonies[8,9]). On the other hand, the motility of artificial microswimmers grows less efficient with increasing density.[15] Without entering the details of the specific perception mechanisms, we can define the sensing function of particle i as follows:[6,20]

$$P_i(\alpha) = \sum_{j\in V_i^\alpha} \frac{1}{2\pi r_{ij}}, \tag{3}$$

where r_{ij} is the distance between particles i and j, and V_i^α denotes the visual cone of particle i, centered around the direction of its self-propulsion velocity, $\boldsymbol{v}_{0i}$, with finite horizon, $r_{ij} \le d_c$. This means that each particle senses the presence of other particles only within a restricted visual cone and a finite distance d_c. For a uniform active suspension of density $\rho_0 = N/\pi R^2$, the sensing function of a particle placed at the center of the cavity reads[5]

$$P_0(\alpha) = (\alpha/\pi)\rho_0 R. \tag{4}$$

We assume now that the particle motility is governed by the following simple *quorum sensing protocol* [Fig. 1(b)],

$$|\boldsymbol{v}_{0i}| = \begin{cases} v_0, & P_i(\alpha) \le P_0(\alpha), \\ 0, & P_i(\alpha) > P_0(\alpha). \end{cases} \tag{5}$$

Clearly, this form of particle interaction is non-reciprocal, since j may be perceived by i and, therefore, influence its dynamics, without being affected by the presence of i. The dynamical implications of the non-reciprocal interactions in biological matter are discussed at length by Bechinger and coworkers in Refs. [5,6]. For an earlier and more elaborated quorum sensing model of synthetic active matter, readers can refer to Ref. [21]. What matters here is that for appropriate choices of the horizon range d_c and the visual angle α, clustering may occur, as illustrated in Fig. 1(c).

Results. The number of tunable parameters of our model is quite large. In our simulations we keep the particle radius r_0 and self-propulsion speed v_0 fixed, amounted to setting space and time units. The particle number N and the cavity radius R play no key role as long as the suspension packing fraction $\phi_0 = N(r_0/R)^2$ is kept sufficiently small (typically $\phi_0 < 0.2$), to avoid steric clustering.[3] We remind that the active-passive transition threshold $P_0(\alpha)$ of Eq. (4) scales like N/R. All remaining parameters D_0, $D_\theta = 1/\tau_\theta$, α, d_c, and λ are varied to shed light on the underlying collective dynamics.

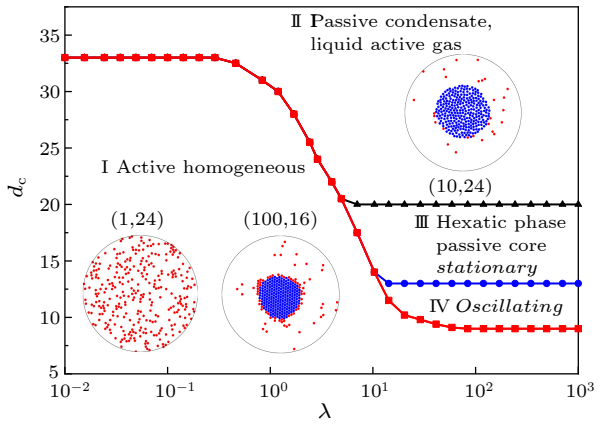

Fig. 2. Phase diagram in the space parameter (λ, d_c). Four distinct regions are distinguishable, namely, I (below the red curve): all particles remain active; Ⅱ: a liquid condensate of passive particle coexists with a gas of active particles; Ⅲ: the passive condensate solidifies into a steady-state hexatic structure; and Ⅳ: periodic formation of hexatic passive clusters (also see Fig. 3). Snapshots of the relevant suspension patterns taken at time $t = 2 \times 10^4$ are shown as insets for different (λ, d_c); red and blue circles denote respectively active and passive particles.

Our main findings are summarized in Fig. 2 for the optimal case of full visual perception $\alpha = \pi$, persistence length $l_\theta = v_0\tau_\theta$ much larger than the cavity diameter, and small translational noise D_0 (whereby the time for a particle to diffuse a distance of the order of its diameter is much larger than to self-propel the same distance). The resulting 2D parameter space (λ, d_c) is traversed by a continuous separatrix curve, d_c vs λ, whereby below (above) it all JPs retain (lose) their active nature. Since the packing fraction of the simulated active suspension is too small to trigger steric clustering, no active aggregates are detected (region I). For small λ values the suspension maintains its initial uniform distribution, whereas at large λ, transient, short-lived active clusters form and dissolve (see Fig. 1 of the Supplemental Material[22])

Above the separatrix curve, the active-passive transitions induced by quorum sensing, Eq. (4), sustain the formation of large clusters, with core consisting of passive particles. For large d_c values, region Ⅱ, one typically observes a large passive condensate surrounded by a low-density gas of active particles [also see the active and passive radial distributions of Fig. 1(d)], which bears a certain similarity with the situation analyzed in Ref. [23]. The passive constituents of the condensate keep fluctuating in thermal noise, as expected in a liquid phase. At large λ, when the wall scatters the colliding particles mostly toward the center of the cavity, the clustering mechanism exhibits additional distinct features. Lowering d_c, we can detect two more regions, Ⅲ and Ⅳ, characterized by very dense clusters made of a passive core surrounded by an active layer; in both of them, the particles are closely packed into hexatic structures.[24] The particles in the cluster active layer show larger motility than in the cluster core, but substantially lower than the surrounding active gas particles, As a major difference, in region Ⅲ the clusters are stationary in time, whereas in region Ⅳ the clusters appear and disappear over time. The time oscillating clustering process of region Ⅳ is further analyzed in Fig. 3. In the top panel there we plot the fraction of passive particles, N_p/N, versus time for $\lambda \to \infty$. One notices immediately that for d_c values corresponding to the regions I–Ⅲ, this ratio approaches a steady state value after a transient of the order of the ballistic cavity crossing time, R/v_0. We also remark for all curves $N_p(t \to \infty)/N < 1$, no matter what is d_c, which suggests that a gas of active particles is always at work. Vice versa, as anticipated above, for system configurations in the region Ⅳ, N_p/N appears to execute persistent irregular time oscillations. A spectral analysis of the time-dependent ratio $N_p(t)/N$ confirms that: (i) $N_p(t)$ fluctuates around a stationary asymptotic value $N_p(\infty) < 1$; (ii) the spectral density of the subtracted ratio, $[N_p(t) - N_p(\infty)]/N$ (an example is shown in the inset of Fig. 3), peaks around a finite frequency of the order of D_θ. We further observe that, with increasing D_θ, region Ⅳ in Fig. 2 shrinks and finally disappears.

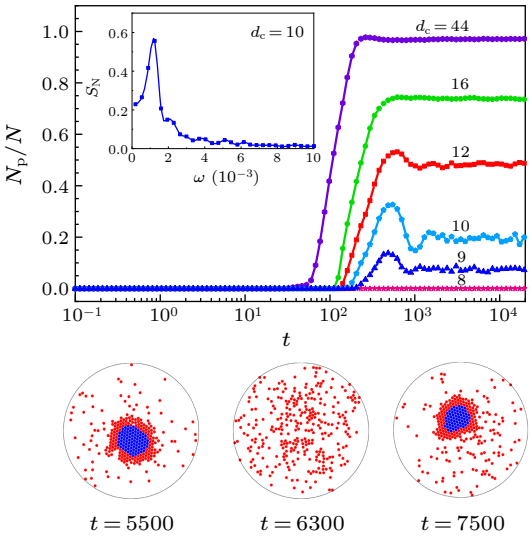

Fig. 3. Cluster stability. Top panel: the fraction of passive particles, $N_p(t)/N$, vs t for different d_c (see legend). The scattering angle distribution here is $p(\phi) = \delta(\phi)$, which corresponds to the limit $\lambda \to \infty$ of Eq. (2). Inset: frequency spectrum of the subtracted function $[N_p(t) - N_p(\infty)]/N$ in the stationary regime for $t \in (2 \times 10^3, 2 \times 10^4)$. Bottom panels: snapshots showing the aggregation and evaporation of a hexatic cluster for $d_c = 10$. In panels, active/passive particles are denoted by red/blue circles and the remaining simulation parameters are $\alpha = \pi$, $D_\theta = 0.001$, $v_0 = 0.5$, $R = 45$, $r_0 = 1$, $N = 304$, and $D_0 = 0.01$.

The numerical results of Figs. 2 and 3 demonstrate the role of the boundary in the cluster formation. At large λ, the distribution of the scattering angle, $p(\phi)$, is mainly peaked around $\phi = 0$; the boundary exerts a lensing effect on the active particles by re-directing them toward the center of the cavity. This clearly enhances the probability that the sensing function, $P_i(\alpha)$, of the particles there overcome the threshold value, $P_0(\alpha)$, of Eq. (4), thus triggering the clustering process. This is the key "herding" function of the gas of active particles continuously bouncing between the cavity and the cluster border. Accordingly, we note that in region Ⅱ the clusters tend to be denser along the border. In the opposite limit of wide scattering angle distribution, i.e., for small λ, the active suspension is no longer focused toward the cavity center and clustering is suppressed. The separatrix curve in Fig. 2 clearly shows that for $\lambda \to 0$ clustering requires that $d_c \sim R$, as implicit in the quorum sensing protocol adopted with Eqs. (3) and (4).

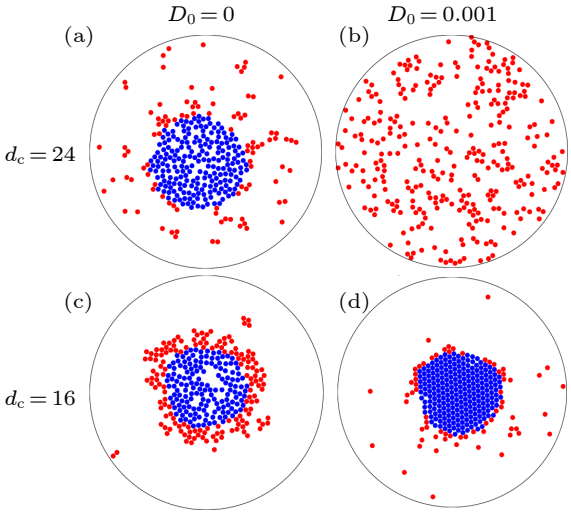

Fig. 4. Role of additive noise. Left panels: $D_0 = 0$ and snapshot time $t = 10^5$; right panels: $D_0 = 0.001$ and $t = 2 \times 10^4$; top panels: $d_c = 24$ and $D_\theta = 0.01$; bottom panels: $d_c = 16$ and $D_\theta = 0.001$. The remaining simulation parameters are $\alpha = \pi$, $v_0 = 0.5$, $R = 45$, $r_0 = 1$, and $N = 304$. The ϕ distribution and the particle color code are the same as in Fig. 3.

Discussion and Conclusions. The phase diagram of Fig. 2 is obtained for a convenient choice of the tunable parameters D_0, D_θ, and α. We now briefly discuss the role of these parameters in the clustering process.

(i) *Role of Spatial Noise, D_0.* The additive noises $\xi_{xi}(t)$ and $\xi_{yi}(t)$ in Eq. (1) keep the particles diffusing even after they undergo the active-to-passive transition. This has a twofold consequence. On the one hand, it hampers the cluster formation by delaying it in time and pushing the separatrix curve of Fig. 2 to higher d_c values [compare Figs. 4(a) and 4(b)]. On the other hand, for $D_0 = 0$ the passive particles come immediately at rest after having reset their self-propulsion velocity to zero. This leads to the buildup of frozen clusters with an amorphous glassy structure [Fig. 4(c)]. Vice versa, adding a little amount of noise allows clusters to rearrange themselves in the denser hexatic structures of region Ⅲ [Fig. 4(d)].

(ii) *Role of Rotational Noise, D_θ.* In Fig. 2 we assume that the particle persistence length $l_\theta = v_0/D_\theta$ is much larger than the cavity diameter. That choice is convenient in that it enhances the role of the boundary dynamics in the clustering process. Indeed, under this condition, active JPs may hit the cavity walls repeatedly before grouping at the center, where eventually undergo the active-to-passive transition. To clarify the role of the persistence time $\tau_\theta = 1/D_\theta$, we simulate the time evolution of the same suspension for increasing values of D_θ and observe that cluster formation gets, indeed, progressively suppressed (see the Supplemental Material [22] for details). This comes as no surprise, since upon increasing D_θ, the persistence length l_θ decreases and the active particles' dynamics resembles more and more standard Brownian motion with strength $v_0^2/2D_\theta$.

(iii) *Role of the Visual Angle, α.* We now consider the cases of $\alpha < \pi$, contrarily to Fig. 2. This means that the neighbor perception of particle i is restricted to a visual cone directed along its instantaneous self-propulsion velocity vector, $\boldsymbol{v}_{0i}$. [5] This enhances the non-reciprocal nature of the particle interactions. As a consequence, the active-passive transitions at the periphery of the forming clusters become more frequent. Indeed, an incoming particle perceives a comparatively much larger neighbor density than a particle moving outward. We remind here that all particles, active and passive alike, keep rotating randomly [third equation in (1)] with correlation time τ_θ. This mechanism tends to destabilize the forming clusters, so that one expects that shrinking the visual cone eventually suppresses clustering. Our simulations confirm this guess, even though the asymptotic value of the ratio $N_p(t)/N$ exhibits a non-monotonic α dependence with a maximum for $\alpha/\pi \gtrsim (3/4)$ (Fig. 5), compared the snapshots for $d_c = 16$ and $\alpha = (7/8)\pi$ in Fig. 1(c) and $\alpha = \pi$ in Fig. 2. We attribute its behavior to the combined effect of the above mechanism and the α dependence of the sensing threshold $P_0(\alpha)$ (see the Supplemental Material [22] for details).

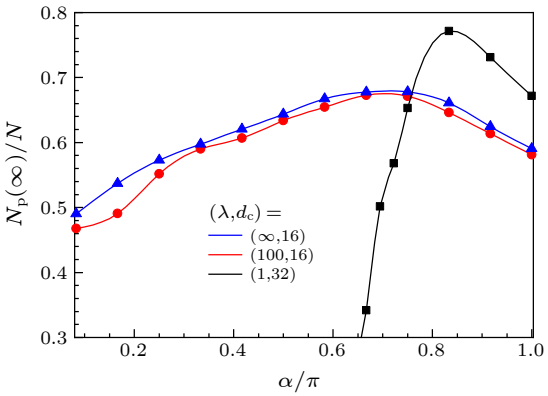

Fig. 5. Role of the visual angle α. Asymptotic value of $N_p(t)/N$ vs α for different choices of the tunable parameters (λ, d_c). The remaining simulation parameters are $D_\theta = 0.001$, $v_0 = 0.5$, $R = 45$, $r_0 = 1$, $N = 304$, and $D_0 = 0.05$.

We conclude this report briefly by discussing a special case, where the cavity wall is replaced by periodic bound-

aries. We consider a square 2D simulation box of size L: particle dynamics and quorum sensing protocols are the same as those for the circular cavity; as a difference, a particle i crossing a box side is re-injected into the box through the opposite side with same self-propulsion vector $\boldsymbol{v}_{0i}$. In this regard, periodic boundaries are reminiscent of the scattering wall of the initial model for $\lambda \to 0$, in that the self-propulsion direction of the re-injected particle tends to be uniformly distributed. Similarly to Fig. 2, one then expects that clustering only occurs for $d_0 \sim L/2$, as a consequence of the very definition of the active-passive transition threshold, $P_0(\alpha)$. Direct numerical simulations (not shown) confirm this expectation.

Acknowledgment. This work was supported by the National Natural Science Foundation of China (Grant Nos. 12375037 and 11935010).

References

[1] Schwarzendahl F J and Mazza M G 2022 *Europhys. Lett.* **140** 47001
[2] Grobas I, Polin M, and Asally M 2021 *eLife* **10** e62632
[3] Fily Y and Marchetti M C 2012 *Phys. Rev. Lett.* **108** 235702
[4] Ginot F, Theurkauff I, Detcheverry F, Ybert C, and Cottin-Bizonne C 2018 *Nat. Commun.* **9** 696
[5] Lavergne F A, Wendehenne H, Bäuerle T, and Bechinger C 2019 *Science* **364** 6435
[6] Bäuerle T, Fischer A, Speck T, and Bechinger1 C 2018 *Nat. Commun.* **9** 3232
[7] Cates M E and Tailleur J 2015 *Annu. Rev. Condens. Matter Phys.* **6** 219
[8] Miller M B and Bassler B L 2001 *Annu. Rev. Microbiol.* **55** 165
[9] Parsek N R and Greenberg E P 2005 *Trends Microbiol.* **13** 27
[10] Tjhung E, Nardini C, and Cates M E 2018 *Phys. Rev. X* **8** 031080
[11] Shi X, Fausti G, Chaté H, Nardini C, and Solon A 2020 *Phys. Rev. Lett.* **125** 168001
[12] Yadzi S and Ardekani A M 2012 *Biomicrofluidics* **6** 044114
[13] Li Y Y, Zhou Y X, Marchesoni F, and Ghosh P K 2022 *Soft Matter* **18** 4778
[14] Ghosh P K, Zhou Y, Li Y, Marchesoni F, and Nori F 2023 *ChemPhysChem* **24** e202200471
[15] Walther A and Müller A H E 2013 *Chem. Rev.* **113** 5194
[16] Ghosh P K, Misko V R, Marchesoni F, and Nori F 2013 *Phys. Rev. Lett.* **110** 268301
[17] Kloeden P E and Platen E 1992 *Numerical Solution of Stochastic Differential Equations* (Berlin: Springer)
[18] Kärger J and Ruthven D M 1992 *Diffusion in Zeolites and Other Microporous Solids* (New York: Wiley)
[19] Codina J, Mahault B, Chaté H, Dobnikar J, Pagonabarraga I, and Shi X 2022 *Phys. Rev. Lett.* **128** 218001
[20] Chen Q, Patelli A, Chaté H, Ma Y, and Shi X 2017 *Phys. Rev. E* **96** 020601(R)
[21] Barberis L and Peruani F 2016 *Phys. Rev. Lett.* **117** 248001
[22] see the Supplemental Material.
[23] Kümmel F, Shabestari P, Lozano C, Volpe G, and Bechinger C 2015 *Soft Matter* **11** 6187
[24] Redner G S, Hagan M F, and Baskaran A 2013 *Phys. Rev. Lett.* **110** 055701